Earth Syst. Dynam., 4, 439–454, 2013
www.earth-syst-dynam.net/4/439/2013/
doi:10.5194/esd-4-439-2013

Earth System Dynamics
Open Access

Do GCMs predict the climate . . . or macroweather?

S. Lovejoy[1], **D. Schertzer**[2], **and D. Varon**[1]

[1]Physics, McGill University, 3600 University St., Montreal, Quebec, Canada
[2]Université Paris Est, Ecole des Ponts Paris Tech, 6–8, Avenue Blaise Pascal Cité Descartes, 77455 Marne-La-Vallee Cedex, France

Correspondence to: S. Lovejoy (lovejoy@physics.mcgill.ca)

Received: 16 October 2012 – Published in Earth Syst. Dynam. Discuss.: 22 November 2012
Revised: 9 October 2013 – Accepted: 21 October 2013 – Published: 28 November 2013

Abstract. We are used to the weather–climate dichotomy, yet the great majority of the spectral variance of atmospheric fields is in the continuous "background" and this defines instead a trichotomy with a "macroweather" regime in the intermediate range from ≈ 10 days to 10–30 yr (≈ 100 yr in the preindustrial period). In the weather, macroweather and climate regimes, exponents characterize the type of variability over the entire regime and it is natural to identify them with qualitatively different synergies of nonlinear dynamical mechanisms that repeat scale after scale. Since climate models are essentially meteorological models (although with extra couplings) it is thus important to determine whether they currently model all three regimes. Using last millennium simulations from four GCMs (global circulation models), we show that control runs only reproduce macroweather. When various (reconstructed) climate forcings are included, in the recent (industrial) period they show global fluctuations strongly increasing at scales $> \approx$ 10–30 yr, which is quite close to the observations. However, in the preindustrial period we find that the multicentennial variabilities are too weak and by analysing the scale dependence of solar and volcanic forcings, we argue that these forcings are unlikely to be sufficiently strong to account for the multicentennial and longer-scale temperature variability. A likely explanation is that the models lack important slow "climate" processes such as land ice or various biogeochemical processes.

1 Introduction

The justification for using GCMs (global circulation models) to model the climate was succinctly expressed by Bryson (1997): "weather forecasting is usually treated as an *initial value* problem . . . climatology deals primarily with a *boundary condition* problem and the patterns and climate devolving there from." The main theoretical criticism of this view is that "nonlinear feedbacks (i.e. two way fluxes) between the air, land, and water eliminate an interpretation of the ocean atmosphere and land atmosphere interfaces as boundaries. . . these interfaces become interactive mediums. . . (that) must therefore necessarily be considered as part of the predictive system" (Pielke, 1998). In addition, from a modelling perspective, we must consider the problem of coupling of "fast" atmospheric processes with a multitude of "slow" climate processes. Some of these (land use, carbon cycle, sea ice) are already incorporated into the more advanced GCMs. However other slow processes – such as land ice, deep ocean currents or various biogeochemical processes – are missing and this probably includes some that have yet to be identified. Finally, GCMs which are realistic for one epoch may not be realistic for another. For example, due to the importance of anthropogenic forcings in the recent period, below we find that the latter become dominant for scales greater than 10–30 yr, whereas in the preindustrial period, the natural forcings and slow processes become dominant only after a somewhat longer period (≈ 100 yr). In the industrial epoch, the GCMs reproduce the (strong) low frequency variability fairly well, whereas in the preindustrial epoch, the (weaker) low frequency variability is poorly reproduced.

While the debate about climate modelling is important, it needs to be informed by empirical evidence. Before reviewing quantitative analyses, consider Fig. 1 that shows examples of temperatures from two scales within the weather regime (0.067 s, 1 h) and at two lower resolutions (top curves, 20 days and 1 century). Other atmospheric fields (wind, humidity, precipitation, etc.) are qualitatively the same at

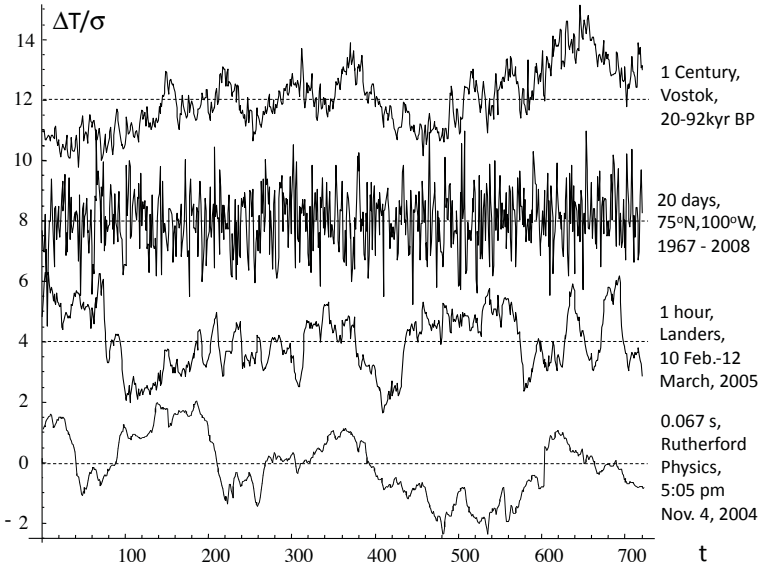

Fig. 1. Dynamics and types of scaling variability: a visual intercomparison displaying representative temperature series from weather, (low frequency) macroweather and climate ($H \approx 0.4$, 0.4, -0.4, 0.4, bottom to top, respectively). To make the comparison as fair as possible, in each case, the sample is 720 points long and each series has its mean removed and is normalized by its standard deviation (0.35, 4.49, 2.59, 1.39 K, respectively), the three upper series have been displaced in the vertical by four units for clarity. The resolutions are 0.067 s, 1 h, 20 days and 1 century, respectively, the data are from 4 m above the top of the roof of the Rutherford physics building (Montreal, Quebec), a weather station in Lander, Wyoming, the 20th century reanalysis and the Vostok Antarctic station, respectively. Note the similarity between the type of variability in the weather and climate regimes (reflected in their scaling exponents). This figure is an adaption of a figure in Lovejoy (2013b).

least up to the limits of instrument data i.e. ≈ 150 yr; for a review, see Lovejoy and Schertzer (2013). We see that the weather curves "wander" up or down resembling a drunkard's walk so that temperature differences typically increase over longer and longer periods. In contrast, the 20 day resolution curve has a totally different character with upward fluctuations typically being followed by nearly cancelling downward ones. Averages over longer and longer times tend to converge, apparently vindicating the conventional idea that "the climate is what you expect"; we anticipate that at decadal or at least centennial scales averages will be virtually constant with only slow, small amplitude variations. However the century-scale curve (top) shows that on the contrary the temperature once again "wanders" in a weather-like manner (quantified in Figs. 2 and 3).

There are thus three qualitatively different regimes – not two. While the high frequency regime is clearly the weather and the low frequency regime the climate, the new "in between" regime was described as a "spectral plateau", then "low frequency weather" and later dubbed "macroweather" since it is a kind of large-scale weather whose statistics are well reproduced by control runs of GCMs (see below); it is not a small-scale climate regime (Lovejoy and Schertzer, 2013). Formally, macroweather may thus be defined as this intermediate regime in which average fluctuations decrease with timescale. The weather–macroweather–climate trichotomy has been confirmed in several composite wide-scale range analyses (Lovejoy and Schertzer, 1986; Pelletier, 1998; Huybers and Curry, 2006b) (see Fig. 2, also Wunsch, 2003) yet the implications have not been widely considered.

If we adopt this trichotomy as an objective basis for categorizing atmospheric dynamics, then a "climate state" is no longer defined by 30 yr averages (a tradition that started in 1935 when the International Meteorological Organization (IMO) adopted the first "climatic normal period" as 1901–1930). Rather, a climate "state" or "normal" is defined as an average over the entire range of scales out to the scale of minimum temperature variability. As we see in Fig. 3, this is 10–30 yr for the industrial period, but closer to 100 yr for the preindustrial period (c.f. the bottom global scale curves and Fig. 5). The traditional 30 yr IMO definition turns out to be roughly a compromise between the preindustrial and industrial timescales. The "climate" is then defined as the variability of climate states/normals at longer timescales.

The object of this paper is to systematically compare the scale by scale variability of GCM outputs with the corresponding variability of various instrumental and proxy data sets in an attempt to answer the question: do GCMs model macroweather, the climate or both? While the analyses of GCMs have not been published elsewhere, several empirical analyses are shown for reference. In the few cases where these are not original to this paper, this is clearly indicated.

This paper is structured as follows. In Sect. 2, we review the methods including some recent results pertinent to the

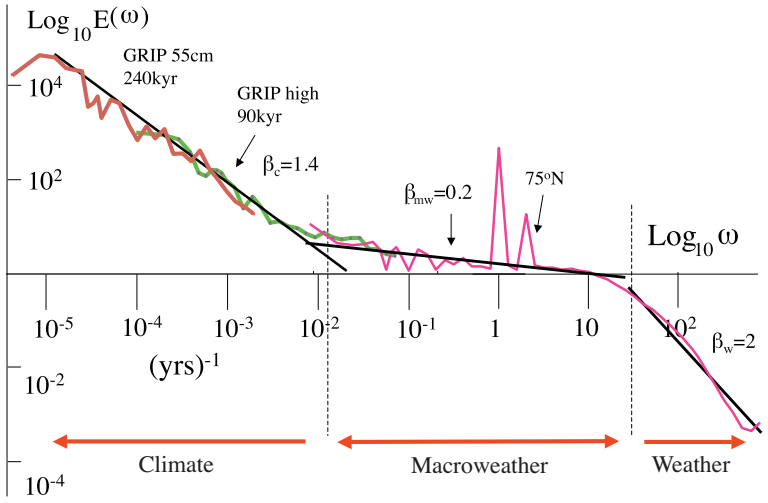

Fig. 2. A composite temperature spectrum: the GRIP (Summit) ice core δ^{18}O, a temperature proxy, low resolution (left, brown) along with the first 91 kyr at high resolution (left, green), with the spectrum of the (mean) 75° N 20th century reanalysis (20CR, Compo et al., 2011) temperature spectrum, at 6 h resolution, from 1871 to 2008, at 700 mb (right). The overlap (from 10–138 yr scales) is used for calibrating the former (moving them vertically on the log–log plot). All spectra are averaged over logarithmically spaced bins, ten per order of magnitude in frequency. Three regimes are shown corresponding to the weather regime with $\beta_w = 2$ (the diurnal variation and harmonic at 12 h are visible at the extreme right). The central low frequency weather "plateau" is shown along with the theoretically predicted $\beta_{mw} = 0.2$–0.4 regime. Finally, at longer timescales (left), a new scaling climate regime with exponent $\beta_c \approx 1.4$ continues to about 100 kyr. Note that a recent revised chronology may modify the very lowest frequencies. Reproduced from Lovejoy and Schertzer (2012b). The black lines are reference lines with the (absolute) slopes indicated.

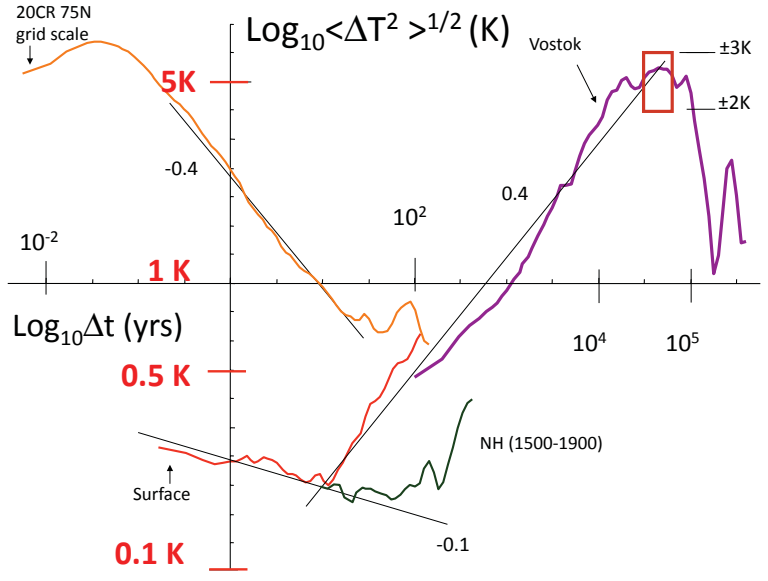

Fig. 3. Empirical RMS temperature fluctuations ($S(\Delta t)$): on the left top we show grid-point-scale (2° × 2°) daily scale fluctuations for both 75° N and globally averaged along with reference slope $\xi(2)/2 = -0.4 \approx H$ (20CR at 700 mb). On the lower left, we see at daily resolution, the corresponding globally averaged structure function. Also shown (bottom) are the average of the three in situ surface series as well as three multiproxy structure functions described in Lovejoy and Schertzer (2012b) (the ensemble average of the RMS fluctuations of the Huang, 2004, Moberg et al., 2005, and Ljundqvist, 2010, multiproxies). The surface curve is the mean of three surface series (NASA GISS, NOAA CDC and HADCRUT3, all 1881–2008). At the right we show the Vostok palaeotemperature series. Also shown is the interglacial "window". This is a simplification of a figure in Lovejoy and Schertzer (2012b).

paper, in Sect. 3 we compare GCM control (unforced) runs and last millennium (forced) runs and in Sect. 4 we conclude.

2 Methods: fluctuations and their statistics

Let us quantify the analysis of Fig. 1 using fluctuations rather than the spectra shown in Fig. 2. Consider a regime where the mean temperature fluctuation $< \Delta T >$ varies as a function of timescale (Δt) as $< \Delta T > \approx \Delta t^H$, where H is the fluctuation (also called "nonconservation") exponent ("$< . >$" indicates statistical averaging). When H>0 fluctuations increase with scale, when $H < 0$, they decrease. To see if this explains the "wandering" and "cancelling" in Fig. 1, we must estimate the fluctuations. Although they are usually defined by the absolute difference ΔT between T at time t and at time $t + \Delta t$:

$$(\Delta T(\Delta t))_{\text{diff}} = |T(t + \Delta t) - T(t)|, \quad (1)$$

this is only sufficient in the "wandering" regime (more precisely, for $0 < H < 1$). An alternative "tendency fluctuation" is useful in the "cancelling" regime (more precisely, for $-1 < H < 0$) and is obtained by simply removing the overall mean $\overline{T}$ and calculating the average of the result:

$$(\Delta T(\Delta t))_{\text{trend}} = \left| \frac{1}{\Delta t} \sum_{t}^{t+\Delta t} T'(t) \right|; \quad T'(t) = T(t) - \overline{T}. \quad (2)$$

To cover both regimes ($-1 < H < 1$) we should instead use the "Haar fluctuation" which is the absolute difference of the mean between t and $t + \Delta t/2$ and between $t + \Delta t/2$ and $t + \Delta t$:

$$(\Delta T(\Delta t))_{\text{Haar}} = \left| \frac{2}{\Delta t} \sum_{t}^{t+\Delta t/2} T(t) - \frac{2}{\Delta t} \sum_{t+\Delta t/2}^{t+\Delta t} T(t) \right|. \quad (3)$$

Technically, this corresponds to defining fluctuations using "Haar" wavelets (rather than for example "poor man's" wavelets which are simply differences (for climate analyses with differences see Lovejoy and Schertzer, 1986). The Haar fluctuation is particularly easy to understand since (with proper "calibration"), in regions where $H > 0$, it can be made very close to the difference fluctuation and in regions where $H < 0$, it can be made close to the "tendency fluctuation". This means that when the mean Haar fluctuations are plotted against scale (Δt), that they can be interpreted either as differences or as averages – depending on whether the fluctuations increase or decrease with scale. While other techniques such as detrended fluctuation analysis (Peng et al., 1994; Kantelhardt et al., 2002; Monetti et al., 2003) perform just as well for determining exponents, they have the disadvantage that their fluctuations (which are standard deviations of the residues of polynomial regressions on the running sum of the original series) are not at all easy to interpret (for a summary see Lovejoy and Schertzer, 2012b and for details see Lovejoy and Schertzer, 2012a).

Beyond the first order (mean) statistics, the variation of the fluctuations with scale can be quantified by their q-th order statistics, the structure function $S_q(\Delta t)$ is particularly convenient:

$$S_q(\Delta t) = \langle \Delta t (\Delta t)^q \rangle. \quad (4)$$

Note that S_q is theoretically defined by an ensemble (statistical) average; in practice we have at most a few realizations – sometimes only a single one – so that the statistics are "noisy". In practice, S_q is estimated as follows. First, at any given scale Δt, the Haar fluctuations ΔT are estimated over all the available disjoint intervals and over all the available realizations. The q-th powers are then averaged (the power $q = 2$ is the only one discussed in this paper, but several values of q are required for a full multifractal analysis; Schertzer and Lovejoy, 2011). The lags Δt are chosen so that there are as close as possible to 20 per order of magnitude in scale (since the lags are integer multiples of the smallest resolution, at the smallest Δt, this is at best only approximate). Finally, in order to better match the difference and tendency fluctuations, the Haar fluctuations were "calibrated" by multiplying them by a factor of 2 (this worked well for all the series analyzed here). Relevant MatLab and Mathematica software are available at http://www.physics.mcgill.ca/~gang/software/index.html.

In a scaling regime, $S_q(\Delta t)$ is a power law; $S_q(\Delta t) \approx \Delta t^{\xi(q)}$, where the exponent $\xi(q) = q\,H - K(q)$ and $K(q)$ characterizes the scaling intermittency (with $K(1) = 0$). In the macroweather regime $K(2)$ is small (≈ 0.01–0.03), so that the RMS (root mean square) variation $S_2(\Delta t)^{1/2}$ (denoted simply $S(\Delta t)$ below) has the exponent $\xi(2)/2 \approx \xi(1) = H$. In the climate regime the intermittency correction is a bit larger (Schmitt et al., 1995) (≈ 0.12) but the error in using this approximation (≈ 0.06) will be neglected.

3 Review of scaling fluctuation analysis on atmospheric data

Although fluctuation analysis is simple to implement and to interpret, it has not been widely applied to climate data, we now give a brief overview. When $S(\Delta t)$ is estimated for various in situ, reanalysis, multiproxy and palaeotemperatures, one obtains Fig. 3 which shows a selection of results from the early reviews (Lovejoy and Schertzer, 2012b, 2013). The key points to note are (a) the three qualitatively different regimes: weather, macroweather and climate with $S(\Delta t)$ respectively increasing, decreasing and increasing again with scale ($H_{\text{w}} > 0$, $H_{\text{mw}} < 0$, $H_{\text{c}} > 0$) and with transitions at $\tau_{\text{w}} \approx 5$–$10$ days and τ_{c}. (b) In the industrial period $\tau_{\text{c}} \approx 10$–$30$ yr (1880–present, Fig. 3, instrumental curve, see also the new analysis in Fig. 5 discussed below) whereas in the preindustrial period, $\tau_{\text{c}} \approx 50$–$100$ yr (1500–1900, Fig. 3, multiproxy curve and the new analysis in

Table 1. Intercomparison of exponents and scales from macroweather (β_{mw}) and climate (β_c) exponents and transition scales from various instrumental/palaeocomposite statistical analyses. The τ_c values in the top two rows are from data north of 30° N and are probably anomalously large.

	β_{mw}	β_c	Local τ_c	Global τ_c
Lovejoy and Schertzer (1986)	< 1 (central England)	1.8 (poles)	≈ 400 yr	≈ 5 yr
Pelletier (1998)	0.5 (continental North America)	1.7 (Antarctica)	≈ 300 yr	–
Huybers and Curry (2006) (tropical sea surface)	0.56 ± 0.08 (NCEP reanalysis)	1.29 ± 0.13 (several different palaeotemperatures)	≈ 100 yr	–
Huybers and Curry (2006) (high latitude continental)	0.37 ± 0.05 (NCEP reanalysis)	1.64 ± 0.04 (several different palaeotemperatures)	≈ 100 yr	–

Fig. 5). This comparison indicates that today, anthropogenic warming dominates the global-scale natural variability for scales $\approx$ 10–30 yr (see Lovejoy, 2013a). (c) The difference between the local- and global-scale fluctuations. (d) The amplitude of the glacial–interglacial (ice age) transition corresponds to overall ± 2 to ± 3 K variations, i.e. $S(\Delta t) \approx 4$ and 6 K, this "glacial–interglacial window" corresponds to half periods of 30–50 kyr. At least in high latitudes, diverse evidence indicates that the $S(\Delta t)$ curve should go through this rectangle.

Note that in scaling regimes, the power spectrum is $E(\omega) \approx \omega^{-\beta}$ (ω is the frequency) with $\beta = 1 + \xi(2) = 1 + 2H - K(2)$ so that ignoring intermittency (i.e. $K(2) \approx 0$), $H > 0$, $H < 0$ correspond to $\beta > 1$, $\beta < 1$ respectively. Hence for macroweather ($\tau_c > \Delta t > \tau_w$); log–log spectra appear as fairly flat "spectral plateaus" (Lovejoy and Schertzer, 1986) (Fig. 2). The present analysis is only of second order ($q = 2$) statistics, a full analysis would be multifractal (all q). However, the intermittency was found to be small (as characterized by $K'(1)$ which was of the order 0.02) so that this will not much change our conclusions.

The scaling composites mentioned in the introduction agree on the basic scaling picture while proposing somewhat different parameter values and transition scales τ_c (Table 1). Studies of macroweather using other techniques (spectra and detrended fluctuation analysis) include those using in situ data (Fraedrich and Blender, 2003; Eichner et al., 2003), sea surface temperatures (Monetti et al., 2003) and ≈ 1000 yr long Northern Hemisphere reconstructions (Rybski et al., 2006) (see also Lennartz and Bunde, 2009 and Lanfredi et al., 2009). Similarly, Huybers and Curry (2006) used NCEP reanalyses and Blender et al. (2006) (see also Franzke, 2010, 2012, who analysed the Holocene's Greenland palaeotemperatures). Finally, multiproxy reconstructions of the Northern Hemisphere (below) yield similar exponents (see Fig. 3 and Lovejoy and Schertzer, 2013).

By considering the fractionally integrated flux models (FIF, i.e. based on cascades, Schertzer and Lovejoy, 1987, 2011; Schertzer et al., 1997) it was argued that whereas in the weather regime, fluctuations depend on interactions in both space and in time, at lower frequencies, only the temporal interactions are important, so that τ_w marks a "dimensional transition". The basic FIF model predicts macroweather exponents to be typically in the range $-0.4 < H < -0.2$ (i.e. $0.2 < \beta < 0.6$) and allows the transition scale τ_w to be estimated theoretically – and essentially from first principles – by first considering Earth's absorbed solar energy and its average rate of conversion into kinetic energy. This yields an estimate close to the empirical tropospheric mean energy flux which is $\varepsilon \approx 10^{-3}$ W kg^{-1}; and which implies a transition scale $\tau_w = \varepsilon^{-1/3} L_e^{2/3} \approx 10$ days ($L_e = 20\,000$ km is the largest distance on Earth; see Lovejoy and Schertzer, 2010, 2012b). The same transition mechanism with $\varepsilon_o \approx 10^{-8}$ W kg^{-1} yields an ocean weather–ocean macroweather transition at about $\tau_{w,o} \approx 1$ yr (roughly as observed; see Lovejoy and Schertzer, 2012b). Finally, theoretical estimates for Mars (taking into account the lower solar irradiance, thinner atmosphere and smaller diameter) yield the predictions $\varepsilon_{w,mars} \approx 0.03$ W kg^{-1} and $\tau_{w,mars} \approx 1.5$ days. This has recently been confirmed using in situ temperature and wind data from the Viking Mars lander (manuscript in preparation); there are thus three examples of weather–macroweather transitions.

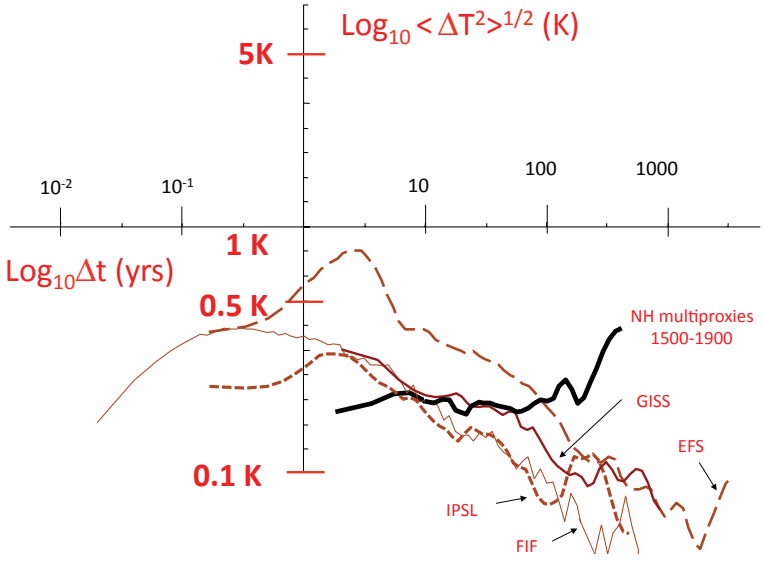

Fig. 4. Control runs versus preindustrial multiproxies: a comparison of the RMS Haar structure functions ($S(\Delta t)$) for temperatures from the multiproxies Fig. 3 (resolution 1 yr, black, 1500–1900) and GCM control runs (brown dashed, IPSL, EFS monthly), annual resolution GISS-E2-R, (thick brown, continuous) and the FIF stochastic model (thin brown). With the exception of the GISS-E2-R (land, Northern Hemisphere), the data are averaged over the entire globe. The IPSL curve is from a 500 yr control run, the EFS is from a 3000 yr control run; the "bump" at 2–4 yr is a broad quasi periodic model artefact. The reference lines have slopes $\xi(2)/2$ so that $\beta = 1 + \xi(2) = 0.2, 0.4, 1.8$. The amplitude of the Haar structure functions have been calibrated using standard and tendency structure functions and are accurate to within ±25 % (a factor 2 was used).

4 Results

4.1 The unforced low frequency variability of GCMs (control runs)

Since in the stable ($H < 0$) macroweather regime fluctuations converge but in the climate regime they diverge, the averages over the whole regime have the lowest possible variability ($S(\Delta t)$) and can be used to define "climate states"; the long-term changes in these states (in the $H > 0$ climate regime) correspond to climate changes. From the point of view of GCM modelling, fixed GCM boundary conditions lead to well-defined GCM climates whereas changing boundary conditions (climate forcings) lead to climate changes. We therefore expect control runs to yield only macroweather with an exponent characterizing the rate at which the model converges to its climate state. This is confirmed in Fig. 4 where we show $S(\Delta t)$ from various GCM control runs, i.e. with constant orbital and solar parameters, no volcanism, constant greenhouse gases and fixed land use for the IPSL model, the more recent Earth Forecasting System (EFS, Jungclaus et al., 2010) and the GISS-E2-R model (from the CMIP5 data base, curated by G. Schmidt; see also Schmidt et al., 2006 and see Table 3 for model details). We see that their fluctuations are decreasing (i.e. in a macroweather-like manner) all the way to their low frequency limits. The challenge for GCMs is therefore to reproduce the growing fluctuations at timescales $> \tau_c$.

Figure 4 also shows $S(\Delta t)$ from the low frequency extension of the stochastic FIF cascade model. These structure functions are compared to the corresponding multiproxy functions, we can clearly see a strong divergence between the empirical and FIF $S(\Delta t)$ for $\Delta t > \approx 10$–30 yr. With the exception of a spurious "bump" at $\Delta t \approx 2$–4 yr scale in the EFS $S(\Delta t)$, the models do a reasonable job at reproducing the average variability between about one month up to $\tau_c \approx 10$–50 yr (depending somewhat on the model and – for GISS-E2-R – the fact that it is for the Northern Hemisphere, land only with therefore somewhat higher variability). However, beyond that, their mean fluctuations continue to decline whereas the empirical $S(\Delta t)$ starts to rise. The grid-scale analyses of the control runs lead us to exactly the same conclusion; indeed the low frequency exponents are all near the same value corresponding to $H \approx -0.4$ ($\beta \approx 0.2$; the global-scale exponents are closer to $H \approx -0.2$, $\beta \approx 0.6$). Figure 4 shows that the GISS-E2-R and IPSL and multiproxy $S(Deltat)$ functions are within $\approx \pm 0.05$ K of each other out to $\Delta t \approx 10$ yr while the EFS model has somewhat larger fluctuations. However at longer timescales, the multiproxy $S(\Delta t)$ strongly diverges from the control runs. Whereas the multiproxy $S(\Delta t)$ at 100 yr is ≈ 0.3 K, and rapidly growing, the IPSL, GISS and EFS $S(\Delta t)$'s are in the range ≈ 0.1–0.2 K and are rapidly decreasing.

These findings are in accord with other studies of the low frequency behaviour of GCMs, including some on "ultra long" (Blender et al., 2006) 10 kyr runs using the detrended

Table 2. Summary of scaling studies of GCM temperatures. All the estimates were made using the DFA method; the spectral exponent β was determined from $\beta = 2\alpha - 1$, where α is the conventional DFA exponent (this expression ignores intermittency corrections).

Reference	Model	Model characteristics	Series length (yr)	Range of scales in analysis	β_{mw}
Fraedrich and Blender (2003) with IPCC scenario IS92a greenhouse gas emissions	ECHAM4/ OPYC	19 levels, T42 OPYC ocean model includes sea ice with rheology	1000 yr	240 yr	≈ 0 continents, ≈ 0.3 coasts, ≈ 1 for oceans
	HadCM3	19 levels, $2.5° \times 3.75°$	1000 yr	240 yr	Same to within ≈ 0.2
Zhu et al. (2006)	GFDL	31 levels, T63	500 yr	500 yr	≈ 1
(preindustrial control runs)	ECHAM5/MPIOM	24 levels, $2° \times 2°$ (land), $1° \times 1°$ (ocean)	500 yr	500 yr	≈ 1 mid-Atlantic overturning
Blender et al. (2006), Fraedrich et al. (2009)	CSIRO atmosphere–ocean model under present-day conditions	9 levels, R 21 horizontal resolution	10 000 yr simulation	3 kyr	0.2–0.8 depending on location
Vyushin et al. (2004) one control simulation, one with historical drivers	ECHO-G = ECHAM4/ HOPE-G	19 vertical levels, T30	1000 yr simulated temperature records	≈ 200 yr	Land 0.2–0.4, ocean 0.4–0.7

fluctuation analysis technique, although these only considered grid-scale statistics which have a transition τ_c at slightly longer timescales than the global ones in Fig. 3 (see Fig. 8). The basic conclusions of the studies have been pretty uniform: the low frequency behaviour was scaling, predominantly with $0 < \beta < 0.6$ (roughly $-0.5 < H < -0.2$, i.e. in the same range as our control runs) and with ocean values a little higher than for land (Table 2). The exponents were robust; for example, with a fixed scenario they were insensitive to the use of different models, in the same model, to the addition of greenhouse gases (Fraedrich and Blender, 2003), or in the last 1000 yr in the Northern Hemisphere, to constant or to historically changing drivers (Rybski et al., 2008). Finally, models with sophisticated sea ice rheology also had similar scaling (Fraedrich and Blender, 2003). In no cases and at no geographical location was there evidence of an end to the macroweather regime. Apparently, the global-scale IPSL, EFS and GISS-E2-R control run analyses in Fig. 3 are typical.

4.2 The last millennium simulations: the climate or macroweather?

If control runs produce only fluctuations decreasing with scale (macroweather), what about forced runs with more realistic low frequency variability? To answer this question, we must systematically compare the model and empirical fluctuations as functions of timescale Δt. However, first we must consider a complication: the effect of anthropogenic forcings over the industrial period. We saw earlier (Fig. 3) that for scales $\Delta t \approx > 10$ yr there was a large difference between the industrial (1880–present) surface series and preindustrial (1500–1900) multiproxies – presumably a consequence of the fact that the recent period variability of the global temperatures is dominated by anthropogenic effects. Figure 5 shows the analysis of eight GISS-E2-R last millennium simulations (Northern Hemisphere, land only) over the period 1880–2005 (CMIP5 database, see also Schmidt et al., 2006, 2011, 2013 and the discussion below). The simulations used solar, land surface and two volcanic reconstructions (Gao et al., 2008; Crowley et al., 2008; hereafter referred to as "Gao" and "Crowley", these are discussed in more detail below). Over the last millennium, orbital changes are too small to be important; the orbital parameters were fixed. Since the

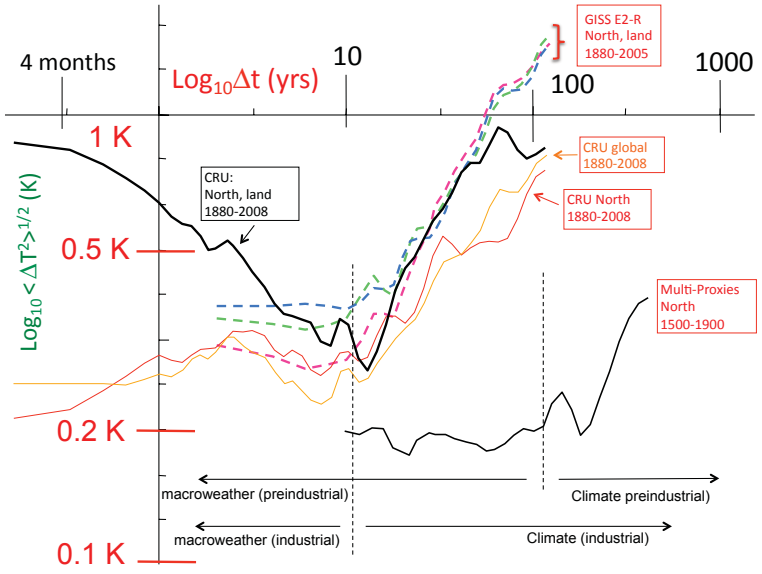

Fig. 5. Recent period instrumental and GCM RMS fluctuations. Comparison of instrumental (CRU, HadCRUT3, black, thick, Northern Hemisphere land only) and GISS-E2-R (dashed: Crowley and Gao volcanic reconstructions (green and blue respectively) and solar only (red); all are for the Northern Hemisphere land only). Gao and Crowley refer to the Gao et al. (2008) and Crowley et al. (2008) volcanic reconstructions discussed in the text. Also shown for reference are the CRU global (orange) and Northern Hemisphere (land and ocean, red) $S(\Delta t)$ for the period 1880–2008. Also shown for reference is the preindustrial multiproxy series (from Fig. 3). Notice that the weather–macroweather transition scale (where the slopes change sign) is roughly 10 yr in the industrial epoch, but closer to 100 yr in the preindustrial epoch (bottom arrows).

differences between the different land use models lead to only small variations, in order to simplify the presentation, we averaged over the three Gao and three Crowley volcanic and the two solar-only runs and compared the results to the Climate Research Unit (CRU) temperature reconstructions (HadCRUT3; Rayner et al., 2006, Fig. 5). It can be seen that over this period, the solar and volcanic forcings only make small differences and that for timescales $\Delta t \approx > 3$ yr, the simulation fluctuation amplitudes all agree quite well with those of the Northern Hemisphere land (however their variability is too weak at shorter times). We conclude that when they are dominated by anthropogenic forcings, the GISS-E2-R simulations have quite accurate variabilities.

We now use the same GISS-E2-R simulations but show the analyses over the preindustrial period, 1000–1900 (Fig. 6). We see that the behaviour is radically different. First, the simulations with the solar forcings only are very close to the control run (indicating that their forcings are quite weak). In contrast, the volcanically forced runs show that the amplitudes are too strong at scales $\Delta t \approx < 100$ yr, but quickly decrease and become too weak for longer Δt. Interestingly, at $\Delta t \approx \tau_c$ (≈ 20 yr) the sign of the volcanic slopes changes. However, the series with volcanic forcings vary in the opposite direction from the data: first constant or growing and then decreasing with scale. When compared with the multiproxies we see that whereas at $\Delta t \approx 10$ yr, the volcanic forcings are factors 2–4 too large, at 400 yr scales they are factors 1.5–4 too small. In contrast, the series with solar only forcing are too weak by a roughly constant factor ≈ 1.5 and ≈ 4 at 10 yr and ≈ 400 yr, respectively. It is interesting to note that these $S(\Delta t)$ are quite close (generally within a factor of 2) to those obtained on outputs of the simplified Zebiak–Cane model published in Mann et al. (2005) (work in progress with C. Varotsos). In conclusion, the GISS-E2-R results are different for the different epochs although only the results of the recent period seem fully realistic.

Focusing on the preindustrial period (here 1500–1900), we considered two other GCMs and their last millennium simulations: the ECHO-G "Erik the Red" simulation (von Storch et al., 2004) and two EFS simulations (Jungclaus et al., 2010). The ECHO-G simulation was chosen because in the IPCC AR4 (Solomon et al., 2007) twelve different millennium simulations were compared (although only two were full GCMs) and it was noted that ECHO-G had significantly stronger low frequency variability than any of the others. Indeed, Osborn et al. (2006) found that, due to initialization problems and lack of sulfates, ECHO-G was only reliable over the period 1300–1900 AD; our range 1500–1900 AD was free of these problems.

In the last 1000 yr, the key preindustrial forcings are volcanic and solar. The EFS, ECHO-G and GISS-E2-R simulations used similar "reconstructed" volcanic forcings; the correct solar reconstructions are much less certain. The amplitudes (i.e. calibration) of the "reconstructed" solar forcings are described in terms of percentages of variation since the 17th century "Maunder minimum". Values of 0.1 % and

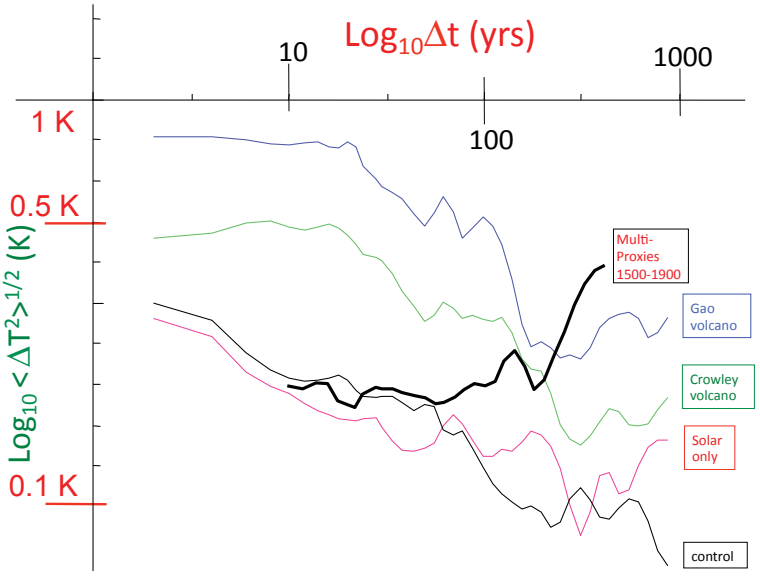

Fig. 6. Preindustrial multiproxy and GISS-E2-R RMS fluctuations. Same as Fig. 5 except for the preindustrial period (1000–1900), the lower black curve is the GISS-E2-R control run from Fig. 4.

0.25 % are considered respectively low and high solar forcing values (see Krivova and Solanki, 2008) for a recent review. In these terms, the ECHO-G forcings were "high" (0.25 %) whereas the EFS simulations were run at both 0.1 and 0.25 % levels. The GISS-E2-R simulations compared both Steinhilber et al. (2009) and Vieira et al. (2011) solar reconstructions corresponding to smaller (0.06 and 0.10 %) variations. Only the pre-1610 part of the reconstructions were based on the ^{10}Be-based reconstructions so that over the range 1500–1900 AD these percentages capture the main solar reconstruction differences (see below and Table 4 for a summary and Fig. 9 for an analysis of some of the forcings).

We have already discussed the GISS-E2-R analyses; for the preindustrial ECHO-G, EFS analyses (Figs. 7 and 8: global- and grid-scales respectively) the key conclusions are the following.

a. The overall EFS variability is very close to the corresponding control run (Fig. 4); it is much too weak.

b. The global-scale low frequency variability (Fig. 7) of the GCM's decrease with increasing Δt and the EFS macroweather behaviour has $S(\Delta t) \approx \Delta t^{-0.4}$.

c. The grid-scale ECHO-G simulation (but not EFS, Fig. 8) has relatively realistic multicentennial variability (close to the multiproxies) with roughly the same τ_c and H as the data and the multiproxies.

These results are quite similar to those obtained from the analysis of the GISS-E2-R simulations discussed earlier. Similarly, Franzke et al. (2013) used spectral analysis and concluded that the ratios of low and high frequency variability of GCMs and palaeodata were significantly different, but they did not specifically consider the macroweather–climate transition, nor did they clearly attribute the problem to a lack of centennial and lower frequency GCM variability.

4.3 Discussion

We reviewed evidence that the variability of the atmosphere out to $\tau_c \approx 10$–30 yr (recent period) and $\tau_c \approx 100$ yr (preindustrial) is dominated by weather and macroweather dynamics. τ_c marks a qualitative transition between a higher frequency regime whose fluctuations decrease with scale ($H < 0$), and the climate regime where they increase with scale ($H > 0$). We showed that control runs of GCMs (studied in the literature and confirmed here) display macroweather regimes converging in power law manner to their "climates" with no low frequency $H > 0$ regime right out to their low frequency limits: as expected, their low frequency variability is too weak. In comparison, starting from scales $\tau_c \approx 10$–30 yr, forced runs during the recent (1880–present) period showed fluctuations in globally averaged temperatures strongly increasing and were quite realistic, i.e. close to the recent period's instrumental global variabilities. Focusing on the preindustrial period – where the multiproxies showed that temperature fluctuations increase after $\tau_c \approx 50$–100 yr – we found (with the partial exception of ECHO-G simulation) that runs forced by solar, volcanic and land use changes had multicentennial variabilities that were too low. Perhaps more significant than these weak amplitudes was the fact that at the largest scales, their fluctuations seemed to be decreasing rather than increasing with lag Δt.

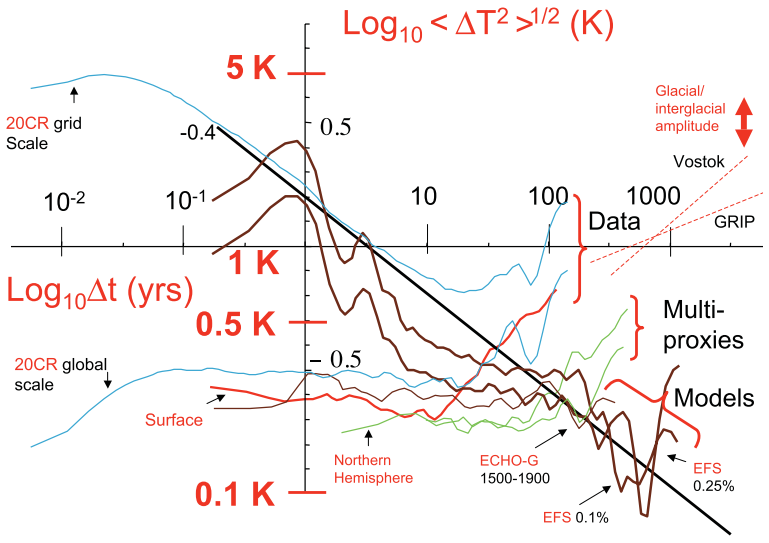

Fig. 7. Pre-1900 forced runs versus data, global scale: this is the same as Fig. 4 (global averages) except that the pre-1900 forced ECHO-G (thin brown) and EFS models (thick brown) are analysed. The upper right dashed lines indicate the rough ranges of the Vostok and GRIP (Greenland ice core) fluctuations at multicentennial scales, and the arrow the glacial–interglacial variations at 50–100 kyr. Also shown are the global- and grid-scale $S(\Delta t)$ from the 20th century reanalysis (blue) as well as two curves for the multiproxies (green) shown in Fig. 3 (the top corresponds to the period 1500–1980, the bottom to the period 1500–1900).

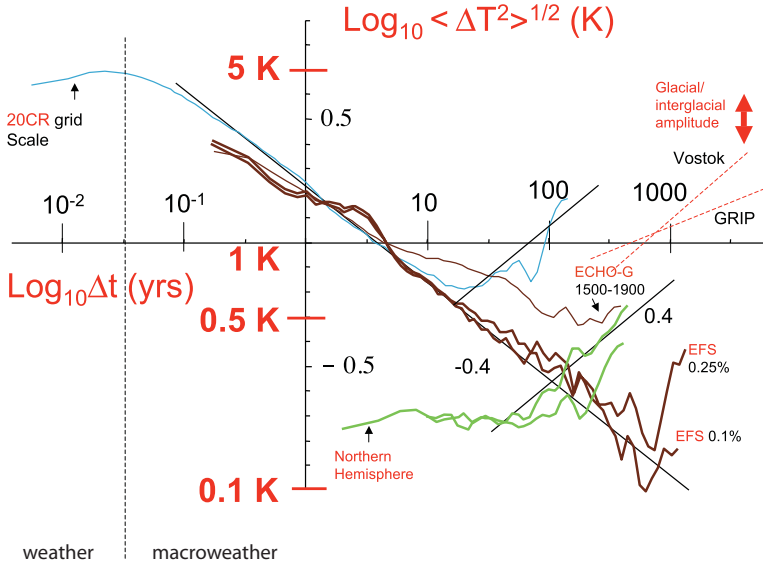

Fig. 8. Grid-scale, forced pre-20th C RMS fluctuations: the same as Fig. 7 except for grid-scale analyses (the green Northern Hemisphere multiproxy curves were added for reference, see Fig. 4). Again, the EFS model has low frequencies that are too weak, but even ECHO-G has weak variability and the low frequency tendency is not clear (i.e. is it starting to rise at $\Delta t \approx 500$ yr?).

Although it seems plausible that if the climate forcing was of the right type and was sufficiently strong a $H > 0$ climate regime would appear, it is not trivial to find the appropriate forcings. This is because in a recent paper (Lovejoy and Schertzer, 2012c), we examined the scale dependence of fluctuations on the radiative forcings (ΔR_F) of several solar and volcanic reconstructions, finding that they generally were scaling with $\Delta R_F \approx A\, \Delta t^{H_R}$ (see Table 4 and Fig. 9 discussed below). Only if $H_R \approx H_T \approx 0.4$, would scale *independent* amplification–feedback mechanisms suffice. For volcanic reconstructions we found $H_{R,vol} \approx -0.3$, which quantifies the obvious fact that while volcanic forcings may be strong on annual scales, their effects rapidly diminish with scale (and this is true even when the observed clustering of volcanic eruptions is taken into account). Since the centennial- and longer-scale temperature fluctuations increase with scale, it

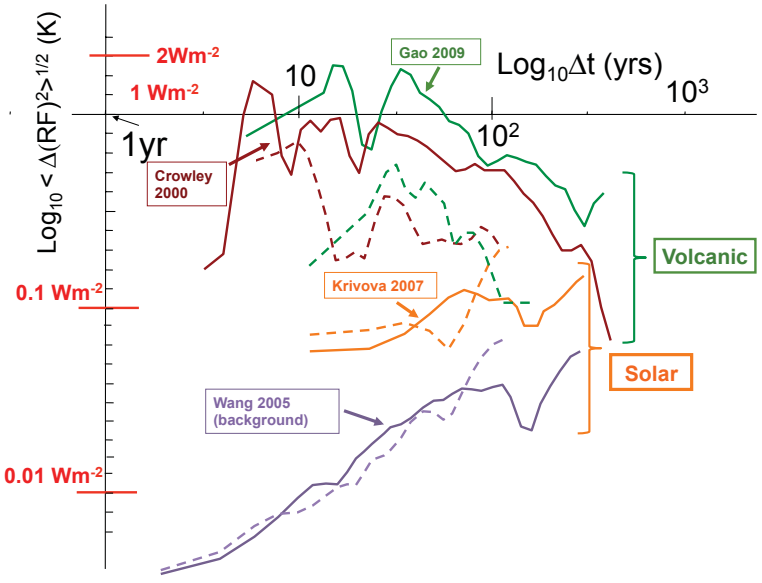

Fig. 9. Radiative forcings from various solar and volcanic reconstructions: a comparison of RMS Haar fluctuations for two solar and two volcanic radiative forcing reconstructions (R_F; units Wm^{-2}). The dashed lines are for the period 1900–present, the solid lines for the period 1500–1900 (volcanic), 1610–1900 (solar). Note that the Wang et al. (2005) curve is only for the background solar forcing (without the 11 yr cycle) whereas the Krivova et al. (2007) curve has a 10 yr resolution. The volcanic series were from reconstructions of stratospheric sulfates using ice core proxies. All the structure functions have been increased by a factor of 2 so that they are roughly "calibrated" with the difference ($H > 0$) and tendency ($H < 0$) fluctuations; see Table 4. The basic forcings have roughly the same scaling properties in the industrial and preindustrial period, only the amplitudes of the volcanic forcings are slightly weaker in the recent epoch.

is unlikely that they can be explained by forcings which decrease with scale. Considering the sunspot-based solar reconstructions, we found $H_{R,sol} \approx +0.4$ hence they grow with scale but, in contrast, the ^{10}Be reconstructions (used for the pre-1610 part of the forcing in the GISS-E2-R simulations) had $H_{R,sol} \approx -0.4$ (decreasing; they cannot both be realistic). While the sunspot-based reconstructions have roughly $H_{R,sol} \approx H_T$ so that they potentially have scale-independent climate sensitivities, if solar forcing was the dominant mechanism for driving the climate at centennial and millennial scales, the amplification/feedback factors would have to be very large: Lovejoy and Schertzer (2012c) estimate that factors $\approx$ 15–20 would be necessary.

Table 4 gives the parameters estimated in Lovejoy and Schertzer (2012c) derived over the entire length of the forcing reconstructions up to the present. However, in Fig. 5 we saw that the decadal- and centennial-scale temperature variability ($S(\Delta t)$) was quite different in the industrial and preindustrial periods. If the industrial solar and/or volcanic forcings were much stronger, then they could potentially explain the anomalously high industrial temperature variability, it is therefore interesting to compare the forcings in the different periods. Figure 9 shows the result for the volcanic forcings (the Gao and Crowley reconstruction discussed earlier, back to 1500) as well as two solar sunspot-based reconstructions (back to 1610 only). Notice that the overall form of the forcings (roughly scaling, linear on log–log plots) is the same for the industrial and preindustrial periods although their amplitudes have changed: the industrial period has slightly weaker (not stronger) volcanic forcings, and roughly unchanged solar forcings. These forcings therefore cannot explain the much larger amplitude (decadal and longer period) industrial-epoch temperature variabilities, the latter are presumably due to the increases in greenhouse gases.

5 Conclusions

The usual idea of the climate is of a regime that is approached as we average over longer and longer periods ("average weather") so that fluctuations are expected to decrease in amplitude and at long enough scales converge to the "climate". By examining GCM control runs – and using a simple-to-interpret real-space fluctuation analysis technique (Haar fluctuations) – we found that beyond weather scales ($\approx$ 10 days), the fluctuations of many GCMs (some analysed here, some in the literature) did indeed have this converging property (albeit with a small exponent so that the convergence is slow). However, both the real world and forced GCMs had a third, lower frequency regime – identified with the true climate – in which fluctuations again begin to increase with scale. In the industrial period, the climate starts at periods of $\approx$ 10–30 yr whereas in the preindustrial period it is closer to 100 yr so that this gives an objective basis – and nuance – for the traditional definition of climate as a 30 yr average.

Table 3. Details of the climate simulations.

Model system	Model components and references	GCM characteristics	Experiment	Series length (yr)
ECHO-G (von Storch et al., 2004)	ECHAM4 (Roeckner et al., 1996), HOPE-G (Wolff et al., 1997)	19 vertical levels, T30, (3.75° resolution)	"Erik the Red", 1000 AD to present, ≈ 0.25 % solar forcing	1000
Earth Forecasting System (EFS) (Jungclaus et al., 2010)	ECHAM5 GCM MPIOM ocean model (Jungclaus et al., 2006), carbon cycle module HAMOCC5 (Wetzel et al., 2006), land surface scheme JSBACH (Raddatz et al., 2007)	19 levels, T31 (3.75° resolution)	Millennium, solar forcing 0.1, 0.25 %, 1000 AD to present	1000 with full forcing, 3000 yr control run
IPSL climate system model: IPSL-CM4	LMDZ GCM (Hourdin et al., 2006), ORCA2 Ocean model, (Madec et al., 1998), LIM Sea ice model (Fichefet and Morales Maqueda, 1997), ORCHIDEE land surface model (Krinner et al., 2005)	19 levels, $2.5° \times 3.75°$ grid	Control run: 1910–2410, for IPCC AR4	500 yr
GISS-E2-R	Includes ocean, tracer and sea ice models, incorporates land use changes, from the CMIP5 data base, curated by G. Schmidt, see also Schmidt et al. (2006, 2011, 2012)	20 levels, $2° \times 2.5°$ grid	8 runs varying forcings, land use	1150 yr (850–2000 AD)

In both epochs the global surface temperature has a minimum RMS fluctuation of about ± 0.1 K (Figs. 3, 5) after which it increases in roughly a scaling manner until attaining from ± 2 to ± 3 K at time periods corresponding to the glacial–interglacial transition (periods of about ≈ 100 kyr, see Fig. 3). While the lower frequency regime was identified with the climate, the middle intermediate regime which was dominated by (coupled ocean–atmosphere) weather processes was termed "macroweather". The challenge of GCMs is therefore to reproduce the slow processes that become dominant at scales between decades and centuries and that remain dominant up to tens of millennia. With the help of the GISS E2-R, we confirmed that the difference between the industrial and preindustrial epochs is a consequence of the fact that in the industrial period the natural forcings (essentially solar and volcanic) are dominated by anthropogenic effects.

The picture that emerges from our analyses of temperatures, reconstructed forcings and model outputs is that of fast weather–ocean processes becoming successively weaker at longer and longer timescales being eventually dominated by new climate processes that become stronger and stronger. These processes presumably include both the responses to external climate forcings (often nonlinearly amplified) as well as low frequency variability generated by new slow climate processes. Elsewhere (Lovejoy and Schertzer, 2012b, c) with the help of palaeotemperature analyses (e.g. Fig. 3), we argued these new responses and processes are apparently dominant from the end of the macroweather regime until scales of ten or more millennia, beyond which orbital forcings are important.

To assess the extent to which current forced GCMs have realistic low frequency variability, we compared the variability of several last millennium simulations with those derived from multiproxy and other palaeotemperature data. We found that the models all show deficits of multicentennial- and millennial-scale variability ($S(\Delta t)$ often about a factor 2 too small at Δt of several centuries). Although the actual deficits of variability are not necessarily very large, they typically decrease with Δt whereas the temperature variability increases with Δt. Orbital forcings are unlikely to be relevant in explaining this increase in variability: their scale dependence was analysed in Lovejoy and Schertzer (2012c) and it was (unsurprisingly) found to be very weak for scales below 10 kyr. This justifies the usual assumption in GCM modelling that changes in the orbital configuration are unimportant over shorter time periods. The main (and usual) candidate for centennial- and millennial-scale forcings are solar and volcanic. However, analysis of various

Table 4. A comparison of various climate radiative forcings (R_F) discussed in Lovejoy and Schertzer (2012c), estimated over the length of time indicated in the fourth column up to the present (Fig. 9 shows industrial and preindustrial analyses for selected series). The exponents were estimated to the nearest 0.1 and the prefactors A are for the formula $\langle(\Delta R_F)^2\rangle^{1/2} = A\,\Delta t^{\xi(2)/2}$ with Δt expressed in years.

Series type	Physical basis	Reference	Series length (yr)	Series resolution (yr)	Scale range analysed (yr)	Prefactor A ($W\,m^{-2}$)	$\xi(2)/2 \approx H_R^*$
Solar	Sunspot-based	Lean (2000)	≈ 400	1	10–400	0.035	0.4
Solar	Sunspot-based	Wang et al. (2005)	≈ 400	1	10–400	0.0074	0.4
Solar	Sunspot-based	Krivova et al. (2007)	≈ 400	10	20–400	0.015	0.4
Solar	TIMS satellite		8.7	6 h	1–8	0.04	0.4
Solar	^{10}Be	Steinhilber et al. (2009)	9300	5 yr smoothed to 40 yr	80–9300	0.4	−0.3
Solar	^{10}Be	Shapiro et al. (2011)	9000	1 yr smoothed to 20 yr	40–9000	3.5	−0.3
Volcanic	Volcanic indices, ice cores, radiance models	Crowley (2000)	1000	1 yr smoothed to 30 yr	60–1000	2.0	−0.3
Volcanic	Ice core sulfates radiance models	Gao et al. (2008)	1500	1 yr smoothed 30 yr	60–1000	2.5	−0.3

* The solar series all have low intermittencies so that $\xi(2)/2 \approx H$ whereas the Crowley and Goa et al. volcanic series have high intermittencies so that $H \approx \xi(2)/2 + C_1 \approx -0.2$, where $C_1 \approx 0.16$ is the intermittency correction.

reconstructions in Lovejoy and Schertzer (2012c) found that these typically become weaker – not stronger – with scale and are unlikely to be strong enough to provide sufficient forcing at multicentennial scales and beyond (see Fig. 9). Therefore, even if the reconstructed solar and volcanic forcings turn out to be unrealistically weak and the true forcing levels are substantially higher, as long as this qualitative (decreasing) character continues to hold, they will still not be able to fully explain the low frequency climate variability. Barring the discovery of a new source of low frequency external forcing, it is hard to escape the conclusion that one must introduce new slow mechanisms of internal climate variability (these might include new internal couplings with existing solar and volcanic forcings). Such new mechanisms must have broad spectra; this suggests that their dynamics involve nonlinearly interacting spatial degrees of freedom. Promising candidates include deep ocean currents, land ice and various biogeochemical processes.

Acknowledgements. We thank G. Schmidt and R. Pielke Sr. for helpful discussions and comments. The public discussion version of the paper also contained useful comments. Anonymous referees of Nature Climate change as well as a GRL editor are thanked for comments on earlier, shorter versions. This work was unfunded; there are no conflicts of interest.

Edited by: A. Kleidon

References

Blender, R., Fraedrich, K., and Hunt, B.: Millennial climate variability: GCM-simulation and Greenland ice cores, Geophys. Res. Lett., 33, L04710, doi:10.1029/2005GL024919, 2006.

Bryson, R. A.: The Paradigm of Climatology: An Essay, B. Am. Meteorol. Soc., 78, 450–456, 2007.

Compo, G. P., Whitaker, J. S., Sardeshmukh, P. D., Matsui, N., Allan, R. J., Yin, X., Gleason, B. E., Vose, R. S., Rutledge, G., Bessemoulin, P., Brönnimann, S., Brunet, M., Crouthamel, R. I., Grant, A. N., Groisman, P. Y., Jones, P. D., Kruger, A. C., Kruk, M., Marshall, G. J., Maugeri, M., Mok, H. Y., Nordli, Ø., Ross, T. F., Trigo, R. M., Wang, X. L., Woodruff, S. D., and Worley, S. J.: The Twentieth Century Reanalysis Project, Q. J. Roy. Meteorol. Soc., 137, 1–28, doi:10.1002/qj.776, 2011.

Crowley, T. J.: Causes of Climate Change Over the Past 1000 Years, Science, 289, 270–273, doi:10.1126/science.289.5477.270, 2000.

Crowley, T. J., Zielinski, G., Vinther, B., Udisti, R., Kreutzs, K., Cole-Dai, J., and Castellano, E.: Volcanism and the Little Ice Age, PAGES Newslett., 16, 22–23, 2008.

Eichner, J. F., Koscielny-Bunde, E., Bunde, A., Havlin, S., and Schellnhuber, H.-J.: Power-law persistance and trends in the atmosphere: A detailed studey of long temperature records, Phys. Rev. E, 68, 046133-40, doi:10.1103/PhysRevE.68.046133, 2003.

Fichefet, T. and Morales Maqueda, M. A.: Sensitivity of a global sea ice model to the treatment of ice thermodynamics and dynamics, J. Geophys. Res., 102, 12609–12646, 1997.

Fraedrich, K. and Blender, K.: Scaling of Atmosphere and Ocean Temperature Correlations in Observations and Climate Models, Phys. Rev. Lett., 90, 108501–108504, 2003.

Fraedrich, K., Blender, R., and Zhu, X.: Continuum Climate Variability: Long-Term Memory, Scaling, and 1/f-Noise, Int. J. Modern Phys. B, 23, 5403–5416, 2009.

Franzke, C.: Long-range dependence and climate noise characteristics of Antarctica temperature data, J. Climate, 23, 6074–6081, doi:10.1175/2010JCL13654.1, 2010.

Franzke, C.: Nonlinear trends, long-range dependence and climate noise properties of temperature, J. Climate, 25, 4172–4183, doi:10.1175/JCLI-D-11-00293.1, 2012.

Franzke, J., Esper, J., and Brönnimann, S.: Spectral biases in tree-ring climate proxies, Nat. Clim. Change, 3, 360–364, doi:10.1038/Nclimate1816, 2013.

Gao, C. G., Robock, A., and Ammann, C.: Volcanic forcing of climate over the past 1500 years: and improved ice core-based index for climate models, J. Geophys. Res., 113, D23111, doi:10.1029/2008JD010239, 2008.

Hourdin, F., Musat, I., Bony, S., Braconnot, P., Codron, F., Dufresne, J.-L., Fairhead, L., Filiberti, M.-A., Friedlingstein, P., Grandpeix, J.-Y., Krinner, G., LeVan, P., Li, Z.-X., and Lott, F.: The LMDZ4 general circulation model: climate performance and sensitivity to parametrized physics with emphasis on tropical convection, Clim. Dynam., 27, 787–813, doi:10.1007/s00382-006-0158-0, 2006.

Huang, S. P., Pollack, H. N., and Shen, P.-Y.: Temperature trends over the past five centuries reconstructed from borehole temperatures, Nature, 403, 756–758, 2000.

Huybers, P. and Curry, W.: Links between annual, Milankovitch and continuum temperature variability, Nature, 441, 329–332, doi:10.1038/nature04745, 2006.

Jungclaus, J. H., Keenlyside, N., Botzet, M., Haak, H., Luo, J.-J., Latif, M., Marotzke, J., Mikolajewicz, U., and Roeckner, E.: Ocean Circulation and tropical variability in the coupled model ECHAM5/MPIOM, J. Climate, 19, 3952–3972, 2006.

Jungclaus, J. H., Lorenz, S. J., Timmreck, C., Reick, C. H., Brovkin, V., Six, K., Segschneider, J., Giorgetta, M. A., Crowley, T. J., Pongratz, J., Krivova, N. A., Vieira, L. E., Solanki, S. K., Klocke, D., Botzet, M., Esch, M., Gayler, V., Haak, H., Raddatz, T. J., Roeckner, E., Schnur, R., Widmann, H., Claussen, M., Stevens, B., and Marotzke, J.: Climate and carbon-cycle variability over the last millennium, Clim. Past, 6, 723–737, doi:10.5194/cp-6-723-2010, 2010.

Kantelhardt, J. W., Zscchegner, S. A., Koscielny-Bunde, K., Havlin, S., Bunde, A., and Stanley, H. E.: Multifractal detrended fluctuation analysis of nonstationary time series, Physica A, 316, 87–114, 2002.

Krinner, G., Viovy, N., De Noblet-Ducoudre, N., Ogeé, J., Polcher, J., Friedlingstein, P., Ciais, P., Sitch, S., and Prentice, I. C.: A dynamic global vegetation model for studies of the coupled atmosphere-biosphere system, Global Biogeochem. Cy., 19, Gb1015, doi:10.1029/2003gb002199, 2005.

Krivova, N. A. and Solanki, S. K.: Models of Solar Irradiance Variations: Current Status, J. Astrophys. Aston., 29, 151–158, 2008.

Krivova, N. A., Balmaceda, L., and Solanski, S. K.: Reconstruction of solar total irradiance since 1700 from the surface magnetic field flux, Astron. Astrophys., 467, 335–346, doi:10.1051/0004-6361:20066725, 2007.

Lanfredi, M., Simoniello, T., Cuomo, V., and Macchiato, M.: Discriminating low frequency components from long range persistent fluctuations in daily atmospheric temperature variability, Atmos. Chem. Phys., 9, 4537–4544, doi:10.5194/acp-9-4537-2009, 2009.

Lean, J. L.: Evolution of the Sun's Spectral Irradiance Since the Maunder Minimum, Geophys. Res. Lett., 27, 2425–2428, 2000.

Lennartz, S. and Bunde, A.: Trend evaluation in records with long term memory: Application to global warming, Geophys. Res. Lett., 36, L16706, doi:10.1029/2009GL039516, 2009.

Ljundqvist, F. C.: A new reconstruction of temperature variability in the extra – tropical Northern Hemisphere during the last two millennia, Geograf. Ann. A, 92, 339–351 doi:10.1111/j.1468-0459.2010.00399.x, 2010.

Lovejoy, S.: Scaling fluctuation analysis and statistical hypothesis testing of anthropogenic warming, Clim. Dynam., submitted, 2013a.

Lovejoy, S.: What is climate?, EOS, 94, 1–2, 2013b.

Lovejoy, S. and Schertzer, D.: Scale invariance in climatological temperatures and the spectral plateau, Ann. Geophys., 4B, 401–410, 1986.

Lovejoy, S. and Schertzer, D.: Towards a new synthesis for atmospheric dynamics: space-time cascades, Atmos. Res., 96, 1–52. doi:10.1016/j.atmosres.2010.01.004, 2010.

Lovejoy, S. and Schertzer, D.: Haar wavelets, fluctuations and structure functions: convenient choices for geophysics, Nonlin. Processes Geophys., 19, 513–527, doi:10.5194/npg-19-513-2012, 2012a.

Lovejoy, S. and Schertzer, D.: Low frequency weather and the emergence of the Climate, in: Extreme Events and Natural Hazards: The Complexity Perspective, edited by: Sharma, A. S., Bunde, A., Baker, D., and Dimri, V. P., AGU monographs, Washington, D.C., 231–254, 2012b.

Lovejoy, S. and Schertzer, D.: Stochastic and scaling climate sensitivities: solar, volcanic and orbital forcings, Geophys. Res. Lett., 39, L11702, doi:10.1029/2012GL051871, 2012c.

Lovejoy, S. and Schertzer, D.: The Weather and Climate: Emergent Laws and Multifractal Cascades, Cambridge University Press, Cambridge, 496 pp., 2013.

Madec, G., Delecluse, P., Imbard, M., and Lévy, C.: OPA 8.1 Ocean General Circulation Model Reference Manual Rep., Laboratoire d'Océanographie DYnamique et de Climatologie, IPSL, Paris, France, 97 pp., 1998.

Mann, M. E., Cane, M. A., Zebiak, S. E., and Clement, A.: Volcanic and solar forcing of the tropical pacific over the past 1000 years, J. Climate, 18, 447–456, 2005.

Moberg, A., Sonnechkin, D. M., Holmgren, K., and Datsenko, N. M.: Highly variable Northern Hemisphere temperatures reconstructed from low- and high-resolution proxy data, Nature, 433, 613–617, 2005.

Monetti, R. A., Havlin, S., and Bunde, A.: Long-term persistance in the sea surface temeprature fluctuations, Physica A, 320, 581–589, 2003.

Osborn, T. J., Raper, S. C. B., and Briffa, K. R.: Simulated climate change during the last 1,000 years: comparing the ECHO-G general circulation model with the MAGICC simple climate model, Clim. Dynam., 27, 185–197, doi:10.1007/s00382-006-0129-5, 2006.

Pelletier, J. D.: The power spectral density of atmospheric temperature from scales of 10** −2 to 10**6 yr, Earth Planet. Sc. Lett., 158, 157–164, 1998.

Peng, C.-K., Buldyrev, S. V., Havlin, S., Simons, M., Stanley, H. E., and Goldberger, A. L.: Mosaic organisation of DNA nucleotides, Phys. Rev. E, 49, 1685–1689, 1994.

Pielke, R.: Climate prediction as an initial value problem, B. Am. Meteorol. Soc., 79, 2743–2746, 1998.

Raddatz, T. J., Reick, C. H., Knorr, W., Kattge, J., Roeckner, E., Schnur, R., Schnitzler, K. G., Wetzel, P., and Jungclaus, J.: Will the tropical land biosphere dominate the climate-carbon feedback during the twenty-first century?, Clim. Dynam., 29, 565–574, 2007.

Rayner, N. A., Brohan, P., Parker, D. E., Folland, C. K., Kennedy, J. J., Vanicek, M., Ansell, T., and Tett, S. F. B.: Improved analyses of changes and uncertainties in marine temperature measured in situ since the mid-nineteenth century: the HadSST2 dataset, J. Climate, 19, 446–469, 2006.

Roeckner, E., Arpe, K., Bengtsson, L., Christoph, M., Claussen, M., Dümenil, L., Esch, M., Giorgetta, M., Schlese, U., and Schulzweida, U.: The atmospheric general circulation model ECHAM-4: model description and simulation of present-day climate Rep., Max-Planck Institute for Meteorology, Hamburg, Germany, 90 pp., 1996.

Rybski, D., Bunde, A., Havlin, S., and von Storch, H.: Long-term persistance in climate and the detection problem, Geophys. Res. Lett., 33, L06718, doi:10.1029/2005GL025591, 2006.

Rybski, D., Bunde, A., and von Storch, H.: Long-term memory in 1000-year simulated temperature records, J. Geophys. Res., 113, D02106, doi:10.1029/2007JD008568, 2008.

Schertzer, D. and Lovejoy, S.: Physical modeling and Analysis of Rain and Clouds by Anisotropic Scaling of Multiplicative Processes, J. Geophys. Res., 92, 9693–9714, 1987.

Schertzer, D. and Lovejoy, S.: Multifractals, Generalized Scale Invariance and Complexity in Geophysics, Int. J. Bifurcat. Chaos, 21, 3417–3456, 2011.

Schertzer D., Lovejoy, S., Schmitt, F., Tchiguirinskaia, I., and Marsan, D.: Multifractal cascade dynamics and turbulent intermittency, Fractals, 5, 427–471, 1997.

Schmidt, G. A., Jungclaus, J. H., Ammann, C. M., Bard, E., Braconnot, P., Crowley, T. J., Delaygue, G., Joos, F., Krivova, N. A., Muscheler, R., Otto-Bliesner, B. L., Pongratz, J., Shindell, D. T., Solanki, S. K., Steinhilber, F. and Vieira, L. E. A.: Present day atmospheric simulations using GISS ModelE: Comparison to in-situ, satellite and reanalysis data, J. Climate, 19, 153–192, doi:10.1175/JCLI3612.1, 2006.

Schmidt, G. A., Jungclaus, J. H., Ammann, C. M., Bard, E., Braconnot, P., Crowley, T. J., Delaygue, G., Joos, F., Krivova, N. A., Muscheler, R., Otto-Bliesner, B. L., Pongratz, J., Shindell, D. T., Solanki, S. K., Steinhilber, F., and Vieira, L. E. A.: Climate forcing reconstructions for use in PMIP simulations of the last millennium (v1.0), Geosci. Model Dev., 4, 33–45, doi:10.5194/gmd-4-33-2011, 2011.

Schmidt, G. A., Jungclaus, J. H., Ammann, C. M., Bard, E., Braconnot, P., Crowley, T. J., Delaygue, G., Joos, F., Krivova, N. A., Muscheler, R., Otto-Bliesner, B. L., Pongratz, J., Shindell, D. T., Solanki, S. K., Steinhilber, F., and Vieira, L. E. A.: Climate forcing reconstructions for use in PMIP simulations of the Last Millennium (v1.1), Geosci. Model Dev., 5, 185–191, doi:10.5194/gmd-5-185-2012, 2012.

Schmidt, G. A., Annan, J. D., Bartlein, P. J., Cook, B. I., Guilyardi, E., Hargreaves, J. C., Harrison, S. P., Kageyama, M., LeGrande, A. N., Konecky, B., Lovejoy, S., Mann, M. E., Masson-Delmotte, V., Risi, C., Thompson, D., Timmermann, A., Tremblay, L.-B., and Yiou, P.: Using paleo-climate comparisons to constrain future projections in CMIP5, Clim. Past Discuss., 9, 775–835, doi:10.5194/cpd-9-775-2013, 2013.

Schmitt, F., Lovejoy, S., and Schertzer, D.: Multifractal analysis of the Greenland Ice-core project climate data, Geophys. Res. Lett., 22, 1689–1692, 1995.

Shapiro, A. I., Schmutz, W., Rozanov, E., Schoell, M., Haberreiter, M., Shapiro, A. V., and Nyeki, S.: A new approach to long-term reconstruction of the solar irradiance leads to large historical solar forcing, Astron. Astrophys., 529, A67, doi:10.1051/0004-6361/201016173, 2011.

Solomon, S., Qin, D., Manning, M., Chen, Z., Marquis, M., Averyt, K., Tignor, M. M. B., and Miller Jr., H. L. (Eds.): Climate Change 2007 The physical science basis, Contribution of Working Group I to the Fourth Assessment Report of the Intergovernmental Panel on Climate Change, Cambridge University Press, Cambridge, 2007.

Steinhilber, F., Beer, J., and Frohlich, C.: Total solar irradiance during the Holocene, Geophys. Res. Lett., 36, L19704 doi:10.1029/2009GL040142, 2009.

Vieira, L. E. A., Solanki, S. K., Krivova, N. A., and Usoskin, I.: Evolution of the solar irradiance during the Holocene, Astron. Astrophys., 531, A6, doi:10.1051/0004-6361/201015843, 2011.

von Storch, H., Zorita, E., Jones, J. M., Dimitriev, Y., Gonzalez-Rouco, F., and Tett, S. F. B.: Reconstructing Past Climate from Noisy Data, Science, 306, 679–682, 2004.

Vyushin, D., Zhidkov, I., Havlin, S., Bunde, A., and Brenner, S.: Volcanic forcing improves Atmosphere-Ocean Coupled, Geophy. Res. Lett., 31, L10206, doi:10.1029/2004GL019499, 2004.

Wang, Y.-M., Lean, J. L., and Sheeley, N. R. J.: Modeling the Sun's magnetic field and irradiance since 1713, Astrophys J., 625, 522–538, 2005.

Wetzel, P., Maier-Reimer, E., Botzet, M., Jungclaus, J. H., Keenlyside, N., and Latif, M.: Effects of ocean biology on the penetrative radiation on a coupled climate model, J. Climate, 19, 3973–3987, 2006.

Wolff, J. O., Maier-Reimer, E., and Legutke, S.: The Hamburg Ocean Primitive Equation Model HOPE Rep., German Climate Computer Center (DKRZ), Hamburg, Germany, 98 pp., 1997.

Wunsch, C.: The spectral energy description of climate change including the 100 ky energy, Clim. Dynam., 20, 353–363, 2003.

Zhu, X., Fraederich, L., and Blender, R.: Variability regimes of simulated Atlantic MOC, Geophys. Res. Lett., 33, L21603, doi:10.1029/2006GL027291, 2006.